Reaction of the Co^{II}-Substrate Radical Pair Catalytic Intermediate in Coenzyme B_{12}-Dependent Ethanolamine Ammonia-Lyase in Frozen Aqueous Solution from 190 to 217 K

Chen Zhu and Kurt Warncke
Department of Physics, Emory University, Atlanta, Georgia 30322

ABSTRACT The decay kinetics of the aminoethanol-generated Co^{II}-substrate radical pair catalytic intermediate in ethanolamine ammonia-lyase from *Salmonella typhimurium* have been measured on timescales of $<10^5$ s in frozen aqueous solution from 190 to 217 K. X-band continuous-wave electron paramagnetic resonance (EPR) spectroscopy of the disordered samples has been used to continuously monitor the full radical pair EPR spectrum during progress of the decay after temperature step reaction initiation. The decay to a diamagnetic state is complete and no paramagnetic intermediate states are detected. The decay exhibits three kinetic regimes in the measured temperature range, as follows. i), Low temperature range, $190 \leq T \leq 207$ K: the decay is biexponential with constant fast (0.57 ± 0.04) and slow (0.43 ± 0.04) phase amplitudes. ii), Transition temperature range, $207 < T < 214$ K: the amplitude of the slow phase decreases to zero with a compensatory rise in the fast phase amplitude, with increasing temperature. iii), High temperature range, $T \geq 214$ K: the decay is monoexponential. The observed first-order rate constants for the monoexponential ($k_{obs,m}$) and the fast phase of the biexponential decay ($k_{obs,f}$) adhere to the same linear relation on an $\ln k$ versus T^{-1} (Arrhenius) plot. Thus, $k_{obs,m}$ and $k_{obs,f}$ correspond to the same apparent Arrhenius prefactor and activation energy ($\log A_{app,f}$ (s^{-1}) = 13.0, $E_{a,app,f} = 15.0$ kcal/mol), and therefore, a common decay mechanism. We propose that $k_{obs,m}$ and $k_{obs,f}$ represent the native, forward reaction of the substrate through the radical rearrangement step. The slow phase rate constant ($k_{obs,s}$) for $190 \leq T \leq 207$ K obeys a different linear Arrhenius relation ($\log A_{app,s}$ (s^{-1}) = 13.9, $E_{a,app,s} = 16.6$ kcal/mol). In the transition temperature range, $k_{obs,s}$ displays a super-Arrhenius increase with increasing temperature. The change in $E_{a,app,s}$ with temperature and the narrow range over which it occurs suggest an origin in a liquid/glass or dynamical transition. A discontinuity in the activation barrier for the chemical reaction is not expected in the transition temperature range. Therefore, the transition arises from a change in the properties of the protein. We propose that a protein dynamical contribution to the reaction, which is present above the transition temperature, is lost below the transition temperature, owing to an increase in the activation energy barrier for protein motions that are coupled to the reaction. For both the fast and slow phases of the low temperature decay, the dynamical transition in protein motions that are obligatorily coupled to the reaction of the Co^{II}-substrate radical pair lies below 190 K.

INTRODUCTION

The molecular mechanisms of the core steps in enzyme catalysis are often veiled by the kinetic complexity and asynchrony of steady-state turnover. Three methods, which involve formation and spectroscopic monitoring of reaction intermediates in solid state samples at cryogenic temperatures, have been developed to study single, or short sequences of, reaction steps in metalloproteins. The first method is the low temperature photodissociation of metal-ligand complexes, for which the archetype is the optically monitored carbon monoxide or dioxygen migration and rebinding to the heme iron in myoglobin (Mb) after photolysis of the carboxy- or oxy-heme state in frozen solutions at temperatures from 10 to 270 K (1,2). This method has been further developed with Mb (3–6), and has been applied to other heme proteins (7–9) and metalloproteins (10,11). The second method is cryoreduction, in which γ-irradiation of a frozen solution sample at 77 K is used to elicit one-electron reduction of a previously redox-poised metal center in the protein (12,13). Graded annealing of the kinetically trapped state is subsequently performed to relax the nonequilibrium, reduced metal center structure, and to thermally activate and step through a portion of the electron transfer or reaction sequence. This protocol has been applied to heme (12–20) and nonheme (21–25) iron proteins. In the third method, which does not involve irradiation, a kinetically unstable enzyme state is prepared and cryotrapped, and then promoted to relax and react by stepwise cycling between the trapping and annealing temperature (26). Here, we report an experiment of the third type, which is distinguished by continuous, full-spectrum electron paramagnetic resonance (EPR) spectroscopic monitoring during the relaxation of the Co^{II}-substrate radical pair intermediate, at the annealing temperature, in coenzyme B_{12} (adenosylcobalamin)-dependent ethanolamine ammonia-lyase (EAL; EC 4.3.1.7; cobalamin (vitamin B_{12})-dependent enzyme superfamily (27,28)) from *Salmonella typhimurium* (29–31). The experiment is aimed at characterizing the molecular mechanistic features of the core reactions of EAL catalysis, and in particular, to distinguish chemical and protein dynamical components of the reaction.

Submitted May 22, 2008, and accepted for publication July 30, 2008.

Address reprint requests to Kurt Warncke, Dept. of Physics, N201 Mathematics and Science Center, 400 Dowman Dr., Emory University, Atlanta, GA 30322. Tel.: 404-727-2975; Fax: 404-727-0873; E-mail: kwarncke@physics.emory.edu.

Editor: Betty J. Gaffney.

0006-3495/08/12/5890/11 $2.00

doi: 10.1529/biophysj.108.138081

The Co^{II}-substrate radical pair accumulates as the only detectable paramagnetic intermediate during steady-state turnover of aminoethanol by EAL (32), and this state can be cryotrapped (33,34). As shown by the minimal mechanism for the catalytic cycle in Fig. 1 (29,30), the process of Co^{II}-substrate radical pair formation begins with binding of aminoethanol (Scheme 1), which triggers the homolytic cleavage of the cobalt-carbon bond in coenzyme B_{12}, yielding low spin, $S = 1/2$ Co^{II} in cobalamin and the proposed $S = 1/2$ 5′-deoxyadenosyl radical. The C5′ radical center of the 5′-deoxyadenosyl abstracts a hydrogen atom from the C1 carbon of the substrate (first hydrogen atom transfer, HT1), which forms 5′-deoxyadenosine and the substrate radical (Scheme 1) (35–37). The substrate radical rearranges to a product radical (Scheme 1) in a detectably irreversible step (38,39). The accumulation of the Co^{II}-substrate radical pair during steady-state turnover on aminoethanol indicates that the radical rearrangement step is at least partially rate-limiting. This has also been shown by substrate $^{14}N/^{15}N$ kinetic isotope effects (40). The product radical reacts by abstracting a hydrogen atom from the C5′-methyl group of 5′-deoxyadenosine (step HT2), which produces a diamagnetic product species and reforms the 5′-deoxyadenosyl radical. After the HT2 step, the 5′-deoxyadenosyl radical recombines with Co^{II} to regenerate the intact coenzyme (41), and products acetaldehyde (Scheme 1) and ammonia are released (42).

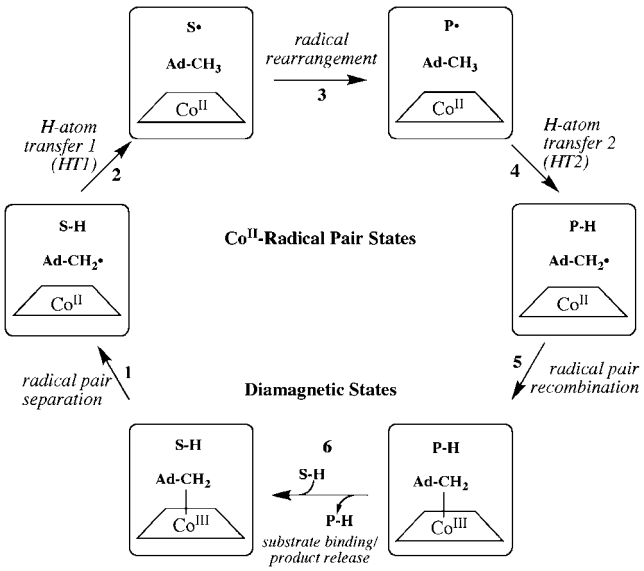

FIGURE 1 Minimal mechanism of catalysis for coenzyme B_{12}-dependent EAL (29,30). The forward direction of reaction is indicated by arrows. The steps are: (*1*) radical pair separation, (*2*) first hydrogen atom transfer (*HT1*), (*3*) radical rearrangement, (*4*) second hydrogen atom transfer (*HT2*), (*5*) radical pair recombination, and (*6*) product release/substrate binding. Substrate-derived species are designated S-H (bound substrate), $S^{\cdot}$ (substrate radical), $P^{\cdot}$ (product radical), and PH (diamagnetic products). The 5′-deoxyadenosyl β-axial ligand is represented as Ad-CH_2 in the intact coenzyme, and as Ad-$CH_2^{\cdot}$ (5′-deoxyadenosyl radical) or Ad-CH_3 (5′-deoxyadenosine) after cobalt-carbon bond cleavage. The cobalt ion and its formal oxidation states are depicted, but the corrin ring and the dimethylbenzimidazole α-axial ligand of the coenzyme (68,69) are not shown for clarity.

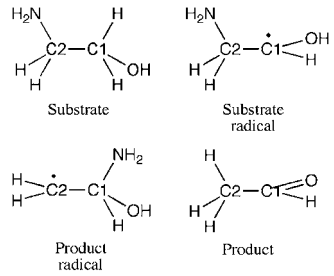

SCHEME 1

In this report, we show that the cryotrapped aminoethanol-derived Co^{II}-substrate radical pair catalytic intermediate in EAL decays to an EPR-silent state upon annealing at $T \geq 190$ K. We have time-resolved the decay after a temperature-step (*T*-step) from a sample holding temperature of 160 or 180 K. The timescale of the decay in the examined temperature range of 190–217 K ($t_{1/2} = 4 \times 10^5$–1×10^3 s, respectively) is slow relative to the instrument dead time ($3.0–6.0 \times 10^1$ s), and the spectrum acquisition period ($1.0–2.0 \times 10^1$ s). The continuous acquisition of EPR spectra during progress of the decay provides the opportunity for the detection and spectroscopic identification of transient paramagnetic intermediates that cannot be addressed at room temperature. The frozen, solid state of the bulk aqueous solvent in the samples restricts product release and substrate binding. Therefore, the decay of the Co^{II}-substrate radical pair state is synchronously initiated by the *T*-step, and the reaction is terminated at the diamagnetic adenosylcobalamin/bound products state. The decay displays monoexponential kinetics from $T = 214$–217 K, but partitions into two distinct monoexponential phases, with decrease in temperature, over the narrow range of $207 < T < 214$ K. The low temperature experiment isolates internal reaction steps for kinetic study and provides a foundation for distinguishing chemical and protein dynamical contributions to enzyme catalysis in EAL.

MATERIALS AND METHODS

Enzyme preparation

Enzyme was purified from the *Escherichia coli* overexpression strain incorporating the cloned *S. typhimurium* EAL coding sequence (43) essentially as described (44), with the exception that the enzyme was dialyzed against buffer containing 100 mM HEPES (pH 7.5), 10 mM potassium chloride, 5 mM dithiothreitol, and 10% glycerol (45). Enzyme activity was determined as described (46) by using the coupled assay with alcohol dehydrogenase/NADH. The specific activity of the purified enzyme with aminoethanol as substrate was 20–30 μmol/min/mg.

Sample preparation

Adenosylcobalamin (Sigma Chemical, St. Louis, MO), 1-^{13}C-aminoethanol and 1,1,2,2-$^{2}H_4$ aminoethanol (Cambridge Isotope Laboratories, Andover,

MA), and natural abundance aminoethanol (Aldrich Chemical, St. Louis, MO) were purchased from commercial sources. The reactions were performed in air-saturated or anaerobic buffer containing 10 mM potassium phosphate (pH 7.5). The anaerobic samples were prepared by using the freeze-pump-thaw procedure, with argon gas backfill. All manipulations were carried out on ice under dim red safe-lighting. The final concentration of enzyme was 10–15 mg/ml, which is equivalent to 20–30 μM for a holoenzyme molecular mass of 500,000 g/mol (44), and an active site concentration of 120–180 μM, based on an active site/holoenzyme stoichiometry of 6:1 (47,48) (K. Warncke, unpublished). Adenosylcobalamin was added to 240–360 μM (twofold excess over active sites).

The Co^{II}-substrate radical pair samples were prepared by using a procedure for fast cryotrapping of steady-state intermediate states in EAL (33). Briefly, after manual mixing of the enzyme-adenosylcobalamin solution with substrate, the sample was loaded into a 4 mm outer diameter. EPR tube, and the tube was plunged into liquid nitrogen-chilled isopentane ($T = 150$ K) to trap the Co^{II}-substrate radical pair state. The total elapsed time from mixing to isopentane immersion was 15 s.

Continuous-wave EPR spectroscopy

EPR spectra were obtained by using a Bruker (Billerica, MA) E500 ElexSys EPR spectrometer equipped with a Bruker ER4123 SHQE cavity. Temperature was controlled with a Bruker ER4131VT liquid nitrogen/gas flow cryostat system, with ER4121VT-1011 evaporator/transfer line, ER4121VT-1013 heater/thermocouple, and 26 liter liquid nitrogen reservoir. For the decay experiments, this temperature control system allowed rapid temperature step changes, relative to the more slowly responding Oxford (Abingdon, UK) ESR900 cryostat, and run times of up to 2–3 $\times$ 10^4 s, depending upon flow rate. Measurements were performed under dim light and with the EPR tubes inserted into the EPR resonator, which shielded the samples from direct exposure to light. Under these conditions with frozen samples, sample degradation owing to coenzyme photolysis is negligible.

Time-resolved EPR measurements

EPR samples were held at a staging temperature of 160 K or 180 K in the ER4131VT cryostat system in the Bruker E560 spectrometer, and the microwave bridge was tuned. *T*-steps from 160 K or 180 K to the decay measurement temperatures of 190, 193, 197, 200, 203, 207, 210, 214, or 217 K were initiated by changing the E4131VT temperature set point. Once the sample temperature stabilized at the set point, the preset auto-tune/auto-scan mode of the spectrometer was triggered, and the sample was auto-tuned at the high temperature set point, followed immediately by continuous spectrum acquisition. The time from initiation of the temperature step to the start of acquisition of the first spectrum was 3.0–6.0 $\times$ 10^1 s. The zero time of the decay was marked at the first collected EPR spectrum. The EPR spectra were acquired with a 24 s sweep time (2.56 ms time constant). The reported temperatures represent the temperature at the sample, which was determined before each decay run by using an Oxford Instruments ITC503 temperature controller with a calibrated model 19180 four-wire resistance temperature detector probe, which has $\pm$0.3 K accuracy over the decay measurement temperature range. For measurements over the temperature range 190–207 K, the ER4131VT cryostat/controller system provided a temperature stability of $\pm$0.5 K over the length of the EPR sample cavity, as measured by using a thermocouple probe that was translated along the EPR tube axis to achieve different heights within a solution sample. The temperature was therefore stable to $\pm$0.5 K during each run. For measurements at 210, 214, and 217 K, the ER4121VT-1011 evaporator/transfer line and ER4121VT-1013 heater/thermocouple were replaced with the standard ER4131VT components, which increased the flow rate of the gas. This led to a more rapid change in temperature during the temperature step, and a desired diminished instrument dead time. Under the faster gas flow in the ER4131VT system, the temperature stability was approximately $\pm$0.7 K over the length of the EPR sample cavity

Kinetic analysis

EPR spectra acquired continuously during the decay were used directly in the kinetic analysis, or were averaged in blocks of from 2 to 20 spectra to increase the signal/noise ratio (SNR), and the acquisition time was calculated as the average time for the block. For each EPR spectrum, the amplitude of Co^{II} was obtained from the difference between the baseline and the peak feature at $g \approx 2.3$, and the substrate radical amplitude was obtained from the difference between peak and trough amplitudes of the derivative feature around $g \approx 2.0$. All data processing programs were written in MATLAB (The Mathworks, Natick, MA). The observed decays were fitted to monoexponential (Eq. 1, $N = 1$) and biexponential (Eq. 1, $N = 2$) functions by using the expression

$$\frac{A(t)}{A(0)} = \sum_{i=1}^{N} A_i e^{-k_i t}, \tag{1}$$

where $(A(t)/A(0))$ is the normalized total amplitude, A_i is the normalized component amplitude ($\sum_{i=1}^{N} A_i = 1$ at $t = 0$), and k_i is the first-order rate constant. The data were also fitted to the power law function, where t_0 and n are adjustable parameters, as given by the expression

$$\frac{A(t)}{A(0)} = \left(1 + \frac{t}{t_0}\right)^{n}. \tag{2}$$

The power law function represents a distribution of monoexponential decay rates (2). The fitting of the kinetics was performed by using Origin (OriginLab, Natick, MA).

Temperature-dependence of the first-order rate constant

The temperature dependence of the first-order rate constant, k, is given by the Arrhenius expression (49)

$$k(T) = Ae^{\frac{-E_a}{RT}}, \tag{3}$$

where E_a is the activation energy, R is the gas constant, and A is a prefactor that represents the value of k as $E_a \rightarrow 0$. In a plot of $\ln k$ versus T^{-1} (Arrhenius plot), the intercept of the linear relation is given by $\ln A$ and the slope is given by $-E_a/R$.

RESULTS

Co^{II}-substrate radical pair EPR spectrum

Fig. 2 shows EPR spectra of the aminoethanol-derived Co^{II}-substrate radical pair. The EPR spectrum of the Co^{II}-substrate radical pair after cryotrapping and before annealing is presented in Fig. S1 of the Supplementary Material (Data S1). The Co^{II} intensity is most prominent in the region around 285 mT, which is near to the $g_\perp = 2.26$ value in the EPR spectrum of isolated cob(II)alamin (50). The Co^{II} transitions extend to the high field edge of the $g_\parallel$ region at 360 mT. The Co^{II} features in the radical pair spectrum are broadened, relative to isolated cob(II)alamin, by the interaction with the unpaired electron localized on C1 of the substrate radical (51). The substrate radical line shape extends from ~325 to 345 mT. The unresolved doublet splitting and inhomogeneous line broadening are caused by the interaction with the unpaired electron spin on Co^{II} (33,51). EPR simulations are able to account for all features in the Co^{II}-substrate radical pair spectrum (52,53).

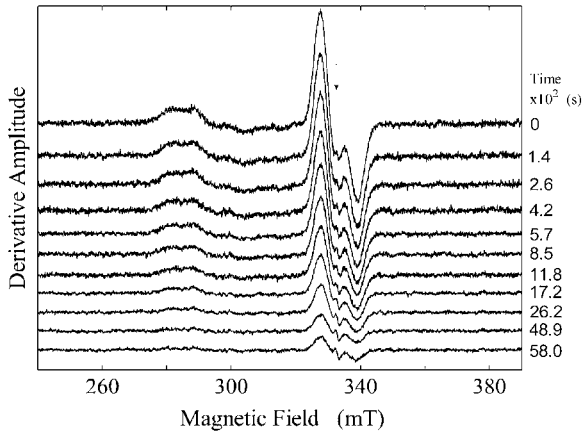

FIGURE 2 Dependence of the EPR spectrum of the Co^{II}-substrate radical pair state in EAL on time after temperature step to $T = 207$ K. The free electron resonance position at $g = 2.0$ is shown by the arrow. Experimental conditions: microwave frequency, 9.3434 GHz; temperature, 207 K; microwave power, 20.25 mW; magnetic field modulation, 1.0 mT; modulation frequency, 100 kHz; scan rate, 6.52 mT/s; and time constant, 2.56 ms.

Time-resolved measurements of EPR spectra during Co^{II}-substrate radical pair decay

EPR spectra were acquired as the decay of the Co^{II}-substrate radical pair progressed at temperatures of 190, 193, 197, 200, 203, 207, 210, 214, and 217 K. Fig. 2 shows a stack plot of a selection of 11 of the 300 total EPR spectra that were collected during the course of a representative decay at 207 K. The Co^{II} and substrate radical EPR signals decay in synchrony (Fig. S2, Data S1). No EPR signals from paramagnetic species other than the Co^{II}-substrate radical pair were detected above the noise level, with the exception of a narrow free radical signal at $g = 2.0$. As reported previously (33), this signal, which corresponds to $<1\%$ of the initial Co^{II}-substrate radical pair amplitude, arises from an organic radical that is formed during the initial sample mixing and cryotrapping procedure. The amplitude of this spurious signal is independent of decay time, and we do not consider it further.

Fig. 3 displays EPR spectra that were acquired in an attempt to observe Co^{II}-radical pair states, other than the Co^{II}-substrate radical pair. Fig. 3 *A* shows normalized EPR spectra acquired at different stages of the Co^{II}-substrate radical pair decay at 197 K. The SNR in these decay spectra was improved by using 1,1,2,2-$^2H_4$-aminoethanol as substrate, which increases the EPR amplitude by threefold relative to natural abundance aminoethanol (33), and by averaging subsets of spectra that correspond to normalized amplitude ranges of 99–90%, 79–70%, and 59–50%. The EPR spectrum of the preannealed sample, collected at 160 K, is also shown in Fig. 3 *A*. The averaged decay spectra are identical to within the noise level, and do not differ significantly from the line shape of the preannealed sample. The SNR relative to the peak-to-trough amplitude of the substrate radical is 2.4–3.0×10^2 for the averaged decay spectra and 3.0×10^2 for the preannealed spectrum. Therefore, no Co^{II}-radical pair species, other than the Co^{II}-substrate radical pair, are detected during the decay at SNR $\approx 10^2$, relative to the peak-to-trough amplitude of the substrate radical.

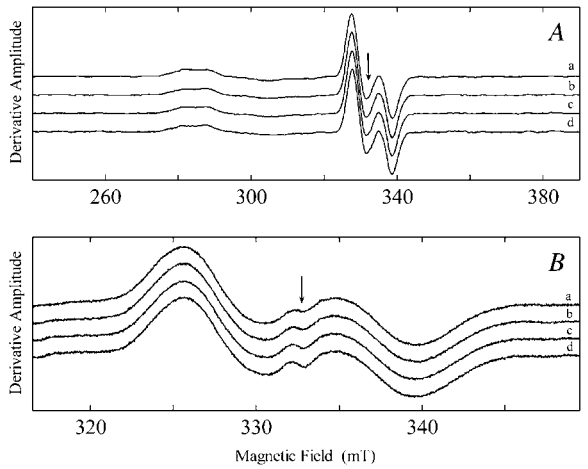

FIGURE 3 Comparison of the EPR spectra of the Co^{II}-substrate radical pair state before annealing and at different levels of decay, for decay performed at $T = 197$ K. (*A*) Co^{II}-substrate radical pair state generated by using 1,1,2,2-$^2H_4$-aminoethanol as substrate. (*a*) Preannealling spectrum, obtained at 160 K. (*b*) Average of spectra corresponding to amplitudes of 99–90% of initial amplitude. (*c*) Average of spectra corresponding to amplitudes of 79–70% of initial amplitude. (*d*) Average of spectra corresponding to amplitudes of 59–50% of initial amplitude. (*B*) Co^{II}-substrate radical pair state generated by using 1-^{13}C-aminoethanol as substrate. (*a*) Preannealling spectrum, obtained at 160 K. (*b*) Average of spectra corresponding to amplitudes of 99–90% of initial amplitude. (*c*) Average of spectra corresponding to amplitudes of 79–70% of initial amplitude. (*d*) Average of spectra corresponding to amplitudes of 59–50% of initial amplitude. Experimental conditions: (*A*) Microwave frequency, 9.3390 GHz; microwave power, 20.25 mW; magnetic field modulation, 1.0 mT; modulation frequency, 100 kHz; scan rate, 6.52 mT/s; and time constant, 2.56 ms. (*B*) Microwave frequency, 9.3390 GHz; microwave power, 20.25 mW; magnetic field modulation, 1.0 mT; modulation frequency, 100 kHz; scan rate, 6.52 mT/s; and time constant, 2.56 ms.

Fig. 3 *B* shows results from the same protocol that was used in Fig. 3 *A*, with the exception that 1-^{13}C-aminoethanol was used as the substrate. Again, the averaged decay spectra are identical to within the noise level, and do not differ significantly from the line shape of the preannealed sample. The 1-^{13}C-label at the C1 radical center increases the substrate radical linewidth by 2.4 mT relative to the natural isotopic abundance radical, owing to the hyperfine interaction of the electron spin with the $I = 1/2$ ^{13}C nucleus (33). If the C2-centered product radical was formed in significant concentration, a narrow line shape would be expected to be superimposed on the substrate radical spectrum. No heterogeneity is observed in the line shapes in Fig. 3 *B*. Therefore, the product radical is not formed in significant concentration during decay of the Co^{II}-substrate radical pair. The absence of detectable paramagnetic species, other than the Co^{II}-substrate radical pair, is consistent with the calculated 5–9 kcal/mol higher free energy of the product radical relative to the substrate radical (54–56), and with the experimentally determined limit on the free energy of the Co^{II}-5′-deoxyadenosyl

radical pair of >3.0 kcal/mol relative to the Co^{II}-substrate radical pair state (57).

Attempt to detect aquocobalamin formed during low temperature Co^{II}-substrate radical pair decay

Single electron transfer-mediated decay of Co^{II}-radical pair intermediates to diamagnetic states in the coenzyme B_{12}-dependent enzymes, lysine 5,6-aminomutase (58), diol dehydratase (59), glutamate mutase (60), and methylmalonyl-CoA mutase (61) has been reported. These single electron transfer reactions occur as a natural consequence of catalysis (58), or because the native course of reaction is altered by mechanism-based inhibitors (59,60) or site-directed mutations in the protein (61). Characteristic features of the electron transfer mechanisms are a monoexponential decay, and formation of the stable, inhibitory enzyme-bound aquocobalamin form of the cofactor. The characteristic ultraviolet absorption band of aquocobalamin (difference extinction coefficient for aquocobalamin minus adenosylcobalamin at $\lambda_{max} = 350$ nm, $\Delta\varepsilon_{350} = 20$ mM^{-1} cm^{-1} (62)) is not detected in the Co^{II}-substrate radical pair samples after the annealing procedure. The monoexponential function also does not fit the decay data for 197–210 K (Fig. S3, Data S1). These results show that the Co^{II}-substrate radical pair recombination reaction is not mediated by a single electron transfer mechanism.

Time and temperature dependence of the substrate radical decay

Fig. 4 shows representative decays of the substrate radical EPR signal as a function of time at temperatures of 197, 200, 203, 207, 210, and 214 K. At the higher temperatures of 207, 210 K, and 214 K, the substrate radical signal is observed to decay fully to zero, to within the noise level. At temperatures below 207 K, the long timescale of the decay, and measuring time limit of 6–8 h, imposed by the cryostat system, preclude recording the decay to the zero level. The kinetic fitting results, described below, are also consistent with the complete decay at all temperatures. The complete decay of the substrate radical EPR amplitude indicates that at least one step in the recombination process can be considered as irreversible.

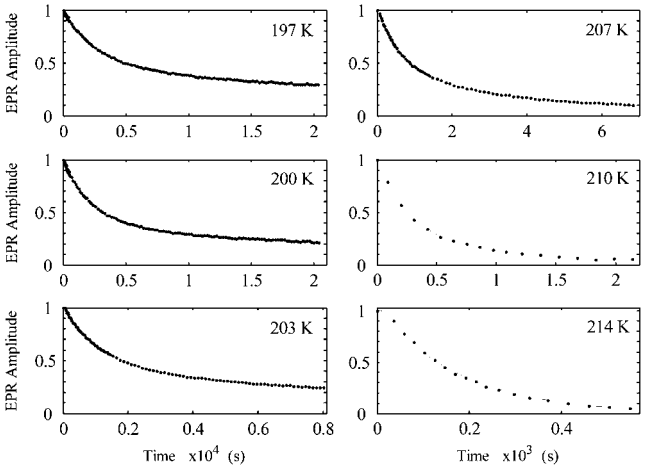

FIGURE 4 Decay of the substrate radical as a function of time at different temperatures from 197 to 214 K, and overlaid best-fit biexponential functions. The EPR experimental conditions are as described in the legend to Fig. 3. The overlaid solid curves correspond to simulations of the decay with a biexponential function (197–210 K) or monoexponential function (214 K). The simulation parameters are presented in Table 1.

The theoretical curves for 197, 200, 203, 207, and 210 K in Fig. 4 represent fits of the data to a biexponential function (Eq. 1, $N = 2$). The biexponential function provides an excellent fit to the decay at all of the temperatures examined from 190 to 210 K. In contrast, the monoexponential decay function (Eq. 1, $N = 1$) provides an unsatisfactory fit to the data obtained at temperatures from 190 to 210 K (Fig. S3, Data S1). The data were also fitted by using the power law function (Eq. 2), which represents a distribution of monoexponential decay rates (2). The heme-carbon monoxide recombination kinetics in Mb at $T < 200$ K have previously been fitted by using the power law function (2). Overall, the power law function gave reasonable fits to the data, but with statistical criteria that were inferior to the biexponential function (Fig. S4, Data S1). Two-temperature annealing experiments, described below, provide evidence against the power law model. The rate constants ($k_{obs,f}$ and $k_{obs,s}$) and normalized amplitude coefficients for the fast and slow phases ($A_{obs,f}$ and $A_{obs,s}$) of the biexponential fitting functions for each temperature are presented in Table 1. The table shows that the rate constants increase with increasing temperature, and that the normalized amplitudes of the fast and slow phases are constant, with average values of 0.57 ± 0.04 and 0.43 ± 0.04, respectively, from 190 to 207 K.

The decay of the Co^{II}-substrate radical pair is well-fit by a monoexponential decay function at 214 K and 217 K. Representative data and fit for 214 K are shown in Fig. 4. The first-order rate constants ($k_{obs,m}$) are presented in Table 1. The results show that, with increasing temperature over the narrow range of $207 < T < 214$ K, there is a transition from a bi- to monoexponential form for the decay.

Distinction between biexponential and power law forms of the Co^{II}-substrate radical pair decay

The distinction between biexponential and power law (multiexponential) functional forms for the Co^{II}-substrate radical pair decay was addressed by a two-temperature annealing protocol. The Co^{II}-substrate radical pair intermediate was annealed at a low temperature to reduce the amplitude to 30–40% of the initial amplitude. The low temperature was selected for this step, because the difference between the fast and slow relaxation times increases with decreasing temperature. This allows preparation of a sample which has a nearly ''pure'' proportion of the slow phase decay component. The sample temperature was then raised to a higher value, and the time dependence of the decay was measured. The decay for a representative two-step annealing experiment performed at 193

TABLE 1 First-order rate constant and amplitude parameters for the fit of the biexponential function to the Co^{II}-substrate radical pair decay kinetics at different temperatures

T (K)	$k_{obs,f}$ (s^{-1})	$A^{*}_{obs,f}$	$k_{obs,s}$ (s^{-1})	$A^{\dagger}_{obs,s}$	$R^{2\ddagger}$
190	6.7×10^{-5}	0.60	5.3×10^{-6}	0.40	0.9994
193	1.2×10^{-4}	0.54	1.3×10^{-5}	0.46	0.9996
197	$3.8(\pm0.1) \times 10^{-4}$	0.56 ± 0.03	$2.4(\pm0.2) \times 10^{-5}$	0.44 ± 0.03	0.9996
200	$5.3(\pm0.6) \times 10^{-4}$	0.55 ± 0.05	$4.1(\pm0.9) \times 10^{-5}$	0.45 ± 0.05	0.9996
203	$8.4(\pm0.6) \times 10^{-4}$	0.58 ± 0.02	$8.0(\pm0.5) \times 10^{-5}$	0.42 ± 0.02	0.9997
207	$1.5(\pm0.1) \times 10^{-3}$	0.61 ± 0.01	$2.4(\pm0.3) \times 10^{-4}$	0.39 ± 0.01	0.9995
210	$4.3(\pm0.8) \times 10^{-3}$	0.56 ± 0.17	$1.5(\pm0.6) \times 10^{-3}$	0.44 ± 0.17	0.9993
214	$5.5(\pm1.6) \times 10^{-3}$	1.00 ± 0.00	—	—	0.9979
217	$1.0(\pm0.3) \times 10^{-2}$	1.00 ± 0.00	—	—	0.9943

*Relative fitted amplitude for the fast phase, normalized to the sum, $A_{obs,f} + A_{obs,s}$.
†Relative fitted amplitude for the slow phase, normalized to the sum, $A_{obs,f} + A_{obs,s}$.
‡R, Pearson's correlation coefficient.

and 207 K is shown in Fig. 5. In contrast to the decay that occurred entirely at 207 K (shown in Fig. 4), the decay of the preannealed sample is well fit by a monoexponential function with a rate constant of 2.3×10^{-4} s^{-1}, which is comparable to the average rate constant of 2.4×10^{-4} s^{-1} obtained for the slow phase of the decay in the biexponential fits of 207 K decays. These results support a biexponential decay, rather than a power law decay, for the temperature range of 190–210 K. Power law decays are characterized by a decrease in rate constant with increasing decay time, and are therefore fit poorly by a single exponential function (2).

DISCUSSION

Temperature dependence of the decay rate constants

Fig. 6 shows a composite Arrhenius plot of the natural logarithms of the observed rate constants (Table 1) for the monoexponential and the fast and slow phases of the biexponential decay as functions of inverse absolute temperature (Eq. 3). The $k_{obs,m}$ and $k_{obs,f}$ values are well-fit by the same linear relation. The $k_{obs,s}$ values for $190 \leq T \leq 207$ K are also well fit by a linear relation that displays different slope and ordinate intercept parameters from the $k_{obs,m}$, $k_{obs,f}$ relation. The $k_{obs,s}$ value for 210 K was not included in the fit, and will be considered below. The adherence of the $k_{obs,m}$ and $k_{obs,f}$ values to the same linear relationship in Fig. 6 indicates that they correspond to the same reaction pathway and rate-limiting step. The different linear relation for $k_{obs,s}$ for $190 \leq T \leq 207$ K suggests that the slow phase of decay either proceeds by a different pathway, or by the same pathway as for the fast phase, but with a different rate-limiting step.

Temperature dependence of the amplitudes of the decay phases

Fig. 7 shows the dependence of the normalized amplitudes of the fast and slow phases of the biexponential decay on temperature. The decay process proceeds with monoexponential kinetics at 217 and 214 K. As the temperature is decreased, the

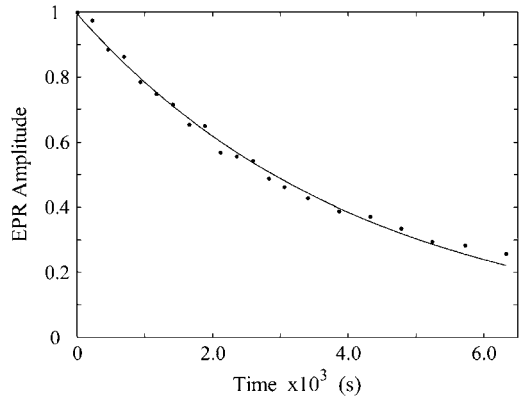

FIGURE 5 Decay of the substrate radical EPR amplitude at 207 K after partial decay at $T = 193$ K. The sample was held at 193 K for 13 h, and the substrate radical amplitude decayed to 38% of the initial amplitude. The subsequent decay at $T = 207$ K is shown, with overlaid monoexponential fit to the data (*solid line*). The EPR experimental conditions are as described in the legend to Fig. 3. Simulation parameters: first-order rate constant, 2.3×10^{-4} s^{-1}; $R^2 = 0.9967$.

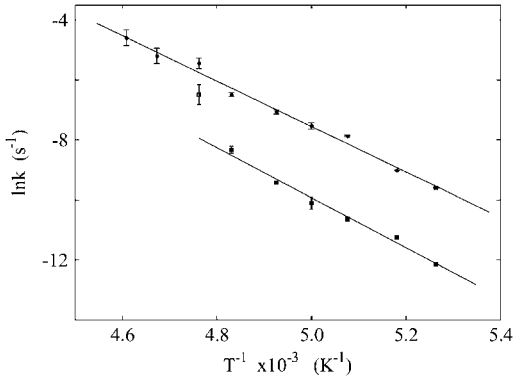

FIGURE 6 Arrhenius plots of the observed first-order rate constants for the decay of the Co^{II}-substrate radical pair, $k_{obs,m}$, $k_{obs,f}$, and $k_{obs,s}$. The combined $k_{obs,m}$ and $k_{obs,f}$ values (*solid circles*) are fitted by the upper line. The $k_{obs,s}$ values corresponding to $190 \leq T \leq 207$ K (*solid squares*) are fitted by the lower line. The $k_{obs,s}$ value for 210 K (*open square*) is not included in the fit. The data are from Table 1. The fitting parameters are presented in Table 2.

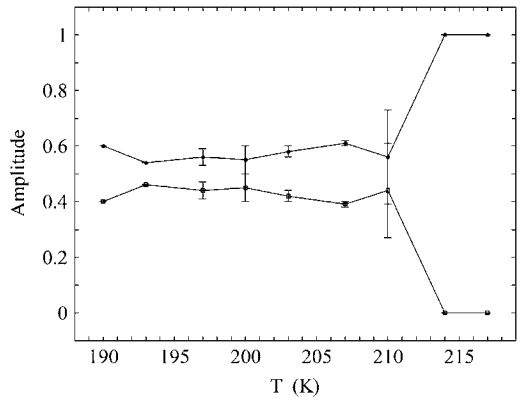

FIGURE 7 Amplitudes of the fast and slow decay phases of the biexponential decay of the Co^{II}-substrate radical pair, $A_{obs,f}$ and $A_{obs,s}$, respectively, as a function of temperature. The amplitudes for 214 and 217 K correspond to the fit to the monoexponential decay function. The curves are drawn to guide the eye. The data are from Table 1.

amplitude of the decay becomes split into the fast and slow components, $A_{obs,f}$ and $A_{obs,s}$, over the relatively narrow temperature range of $207 < T < 214$ K. This range includes the data point at 210 K. Below 210 K ($190 \leq T \leq 207$ K), the normalized fractions of the fast and slow component amplitudes remain constant, with values of $A_{obs,f} = 0.57 \pm 0.04$ and $A_{obs,s} = 0.43 \pm 0.04$, respectively. The constant amplitudes of $A_{obs,f}$ and $A_{obs,s}$ at $T \leq 207$ K, shown in Fig. 7, and the linear Arrhenius relations for the corresponding rate constants, $k_{obs,f}$ and $k_{obs,s}$, in Fig. 6, imply that the two decay components are characterized by different, constant values of the apparent Arrhenius parameters, $E_{a,app}$ and A_{app}, at $T \leq 207$ K. The Arrhenius parameters are ''apparent'', because the rate limitation on the observed reaction may arise from more than one step.

Kinetic mechanism for the Co^{II}-substrate radical pair decay

Low temperature range

The biexponential decay of the Co^{II}-substrate radical pair state for $190 \leq T \leq 207$ K could arise from a homogenous process (single Co^{II}-substrate radical pair population decaying by the same mechanism) or from an inhomogeneous process (two populations of Co^{II}-substrate radical pair states that decay by different mechanisms). The minimal kinetic mechanism for a homogeneous biexponential decay is the two-step, three-state mechanism shown in Scheme 2. The experimental decay data, which correspond to the normalized amplitude, $[A_1]_t/[A_1]_0$, in Scheme 2, has been simulated by using the homogeneous two-step decay model (Eqs. S1–S5, Data S1), and the best-fit k_{ij} and λ_i parameters have been used to predict the values of $[A_2]_t/[A_1]_0$ and $[A_3]_t/[A_1]_0$. Fig. 8 shows a representative simulation of the Co^{II}-substrate radical pair decay for $T = 207$ K. An excellent fit to the decay curve is obtained. However, the simulation predicts a maximum value of 0.5 for $[A_2]_t/[A_1]_0$, and simulations for the decay obtained at the other temperatures also predict $[A_2]_t/[A_1]_0$ values with maxima of ~0.5. The relatively large maximum values of $[A_2]_t/[A_1]_0$ are required by the biexponential nature of the decay, which, in the homogeneous model, implies the transient accumulation of the intermediate A_2 state. The large predicted $[A_2]_t/[A_1]_0$ values are inconsistent with the absence of detectable paramagnetic intermediates in the samples (Figs. 2 and 3), other than the Co^{II}-substrate radical pair. Therefore, we conclude that the Co^{II}-substrate radical pair decay at $T \leq 207$ K is inhomogeneous. Two independent, parallel decay processes exist, which correspond to a fast decay population (state A_f) and a slow decay population (state A_s) of Co^{II}-substrate radical pairs, with the respective observed first-order rate constants, $k_{obs,f}$ and $k_{obs,s}$.

$$A_1 \underset{k_{21}}{\overset{k_{12}}{\rightleftharpoons}} A_2 \underset{k_{32}}{\overset{k_{23}}{\rightleftharpoons}} A_3$$

SCHEME 2

Transition temperature range

The transition from biexponential to monoexponential behavior with increasing temperature occurs in the interval,

TABLE 2 Apparent Arrhenius reaction rate parameters for the fast and slow components of the Co^{II}-substrate radical pair decay

Component	$\log[A_{app}\ (s^{-1})]$	$E_{a,app}$ (kcal mol^{-1})	R^2*
Fast	13.0 (±0.4)	15.0 (±0.6)	0.9909
Slow	13.9 (±0.9)	16.6 (±1.0)	0.9867

*R, Pearson's correlation coefficient.

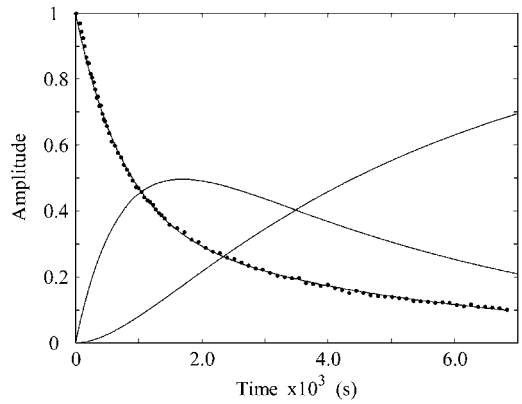

FIGURE 8 Simulation of the Co^{II}-substrate radical decay at 207 K by using the homogeneous linear two-step model (Scheme 2). The experimental decay data are shown as dots. The simulated normalized population of the A_1 ($[A_1]_t/[A_1]_0$, *dotted line*) state, and the calculated time dependence of the A_2 ($[A_2]_t/[A_1]_0$, *solid line*) and A_3 ($[A_3]_t/[A_1]_0$, *dashed line*) states, are shown. Simulation parameters: initial normalized populations $A_{1,0} = 1.0$, $A_{2,0} = A_{3,0} = 0$; $k_{12} = 9.73 \times 10^{-4}\ s^{-1}$, $k_{21} = 3.87 \times 10^{-4}\ s^{-1}$, $k_{23} = 3.09 \times 10^{-4}\ s^{-1}$, $k_{32} = 0\ s^{-1}$ (fixed); and $R^2 = 0.9994$.

$207 < T < 214$ K. Only the 210 K parameter set falls in the transition temperature range. Fig. 6 shows that the data point for $k_{obs,s}$ at 210 K lies significantly above the linear Arrhenius relation that fits the $k_{obs,s}$ data from the low temperature range. The value for $k_{obs,s}$ at 210 K in Table 1 (1.5×10^{-3} s^{-1}) is 3.5-fold higher than predicted by using the low temperature Arrhenius relation (4.3×10^{-4} s^{-1}). Therefore, the data at the single temperature of 210 K suggest that the transition from biexponential to monoexponential decay with increasing temperature is associated with a super-Arrhenius temperature dependence of $k_{obs,s}$. We propose that $k_{obs,s}$ approaches $k_{obs,f}$ as the temperature is increased through the transition region, and therefore, that $E_{a,app,s}$, $A_{app,s}$ approaches $E_{a,app,m/f}$, $A_{app,m/f}$. We also considered an alternative mechanism of an equilibrium, which is highly sensitive to temperature in the transition range, between two populations of Co^{II}-substrate radical pairs, which decay with parameters, ($E_{a,app,s}$, $A_{app,s}$) and ($E_{a,app,m/f}$, $A_{app,m/f}$), respectively. Simulations based on this mechanism gave poor fits to the decay data at 210 K. A finer temperature sampling interval, lower measuring temperature uncertainty, and two-temperature experiments ($T_{low} = 193$ K, $T_{high} = 208$–213 K), such as presented in Fig. 5, will be used to further characterize the temperature dependence of $k_{obs,s}$ (alone, in the absence of interference from the fast phase), to gain further insight into the mechanism of the transition.

High temperature range

The monoexponential decay at $T \geq 214$ K (Figs. 6 and 7, Table 1) is consistent with the increase of $k_{obs,s}$ to the limiting value of $k_{obs,m}$, $k_{obs,f}$ over the range $210 < T < 214$ K. At $T \geq 214$ K, the decay channel represented by $k_{obs,s}$ is absent, and all of the decay of the Co^{II}-substrate radical pair proceeds through a single channel, which is characterized by the Arrhenius parameters, $A_{app,m} = A_{app,f}$ and $E_{a,app,m} = E_{a,app,f}$.

Physical interpretations of the origins of the decay phases

Fast biexponential phase and monoexponential decay processes

The steady-state accumulation, and subsequent cryotrapping, of the Co^{II}-substrate radical pair as the only detectable paramagnetic intermediate, suggest that the step after Co^{II}-substrate radical pair formation is at least partially rate limiting for steady-state turnover. The step after Co^{II}-substrate radical pair formation in the catalytic sequence is the radical rearrangement, which involves conversion of the substrate radical to the product radical (Step 3 in Fig. 1). Partial rate limitation of steady-state turnover by the amine nitrogen-associated radical rearrangement step has also been concluded from substrate $^{15}N/^{14}N$ kinetic isotope effects on k_{cat}/K_M (40). Extrapolation of the linear Arrhenius relation for $k_{obs,f}$ and $k_{obs,m}$ to 298 K gives a value for the decay rate constant of 1.1×10^2 s^{-1} (uncertainty range: 1.4×10^1–8.0×10^2 s^{-1}). This value is consistent with k_{cat} values of 3.0–8.0×10^1 s^{-1} per active site that have been reported for EAL (40,63), and to the rate of decay of the Co^{II}-radical pair state to products after substrate depletion (63–65), in room temperature steady-state kinetic experiments. Studies of the hydrogen atom transfer-mediated exchange of ^3H between [^{3}H]adenosylcobalamin labeled at the C5′ methylene carbon and aminoethanol in EAL show no detectable ^3H equilibration with the free substrate (38,39). Therefore, the reaction of the Co^{II}-substrate radical pair through the reverse of the first hydrogen atom transfer (*HT1*, Step 2 in Fig. 1) is strongly disfavored, and the radical rearrangement step is effectively irreversible (38,39). Therefore, we assign the observed rate constants for the fast phase of the biexponential decay (190–210 K) and the monoexponential decay (214, 217 K) to the native ''forward'' reaction of the substrate radical, through the rearrangement reaction.

Slow biexponential phase

We also assign the observed rate constants for the slow phase of the biexponential decay (190–210 K) to the native ''forward'' reaction of the substrate radical, for the reasons described in the previous section. The 210 K data point suggests a super-Arrhenius increase in $k_{obs,s}$ with increasing temperature, and, therefore a change in the potential energy surface for the slow phase in the transition region. The larger uncertainties in the A_{obs} values for 210 K relative to the low temperature range (Table 1) are consistent with a sharp transition near 210 K that lies partially within the temperature control uncertainty of ± 0.7 K at this temperature (see Methods). The reaction chemistry itself is unlikely to display a mechanistic discontinuity over this temperature range, and therefore, the transition arises from a change in the properties of the protein. A change in the potential energy surface over the relatively narrow temperature range is characteristic of a liquid-glass transition (66). Different proteins display a solvent-dependent, liquid-glass-like transition, or ''dynamical transition'', within the temperature range of 180–220 K (67). The slow phase emerges in association with this transition. We propose that a protein dynamical contribution to the reaction of the substrate radical, which is present above the transition temperature (for example, a fluctuation to a conformation that interacts more favorably with the product radical), is lost below the transition temperature, owing to an increase in the activation energy barrier for protein motions that are coupled to the reaction.

Anharmonic protein motions are observed to be restricted below the dynamical transition temperature (67). The dynamical transition alters the kinetics of reactions that are coupled to the protein motions (67). The transition over $207 < T < 214$ K in EAL appears to be different from this ''classical'' protein dynamical transition, because a parallel,

mechanistically distinct decay path (the slow phase) emerges as the temperature decreases in a fraction of the population, and both the fast and slow phase decay reactions are observed to continue with further decrease in temperature along temperature-independent potential energy surfaces (temperature independent A_{app}, $E_{a,app}$) with monoexponential kinetics, rather than the multiexponential (distributed) kinetics that are characteristic of diatomic molecule migration and recombination with iron in Mb and other heme proteins below the dynamical transition (2, 67). For both the fast and slow phases of the low temperature decay of the Co^{II}-substrate radical pair, the dynamical transition in coupled protein motions that are obligatory for the reaction of the Co^{II}-substrate radical pair lies below 190 K.

SUPPLEMENTARY MATERIAL

To view all of the supplemental files associated with this article, visit www.biophysj.org.

The Supplementary Material includes the EPR spectrum of the Co^{II}-substrate radical pair before annealing, comparison of the decay kinetics of the Co^{II} and substrate radical components of the radical pair EPR lineshape, monoexponential and power law decay function fits to the Co^{II}-substrate radical pair decay at selected temperatures, and expressions from the linear, three-state, two-step decay mechanism that were used for simulation of the homogeneous decay model.

This project was supported by grant No. R01DK054514 from the National Institute of Diabetes and Digestive and Kidney Diseases. The content is solely the responsibility of the authors and does not necessarily represent the official views of the National Institute of Diabetes and Digestive and Kidney Diseases or the National Institutes of Health. The purchase of the Bruker E500 EPR spectrometer was supported by grant No. RR17767 from the National Center for Research Resources of the National Institutes of Health and by Emory University.

REFERENCES

1. Gibson, Q. H. 1956. An apparatus for flash photolysis and its application to the reactions of myoglobin with gases. *J. Physiol.* 134: 112–122.
2. Austin, R. H., K. W. Beeson, L. Eisenstein, H. Frauenfelder, and I. C. Gunsalus. 1975. Dynamics of ligand binding to myoglobin. *Biochemistry.* 14:5355–5373.
3. Frauenfelder, H., P. W. Fenimore, and B. H. McMahon. 2002. Hydration, slaving and protein function. *Biophys. Chem.* 98:35–48.
4. Fenimore, P. W., H. Frauenfelder, B. H. McMahon, and F. G. Parak. 2002. Slaving: Solvent fluctuations dominate protein dynamics and functions. *Proc. Natl. Acad. Sci. USA.* 99:16047–16051.
5. Fenimore, P. W., H. Frauenfelder, B. H. McMahon, and R. D. Young. 2004. Bulk-solvent and hydration-shell fluctuations, similar to alpha- and beta-fluctuations in glasses, control protein motions and functions. *Proc. Natl. Acad. Sci. USA.* 101:14408–14413.
6. Dantsker, D., U. Samuni, J. M. Friedman, and N. Agmon. 2005. A hierarchy of functionally important relaxations within myoglobin based on solvent effects, mutations and kinetic models. *Biochim. Biophys. Acta.* 1749:234–251.
7. Frauenfelder, H., F. Parak, and R. D. Young. 1988. Conformational substates in proteins. *Annu. Rev. Biophys. Biophys. Chem.* 17:451–479.
8. Tetreau, C., L. Mouawad, S. Murail, P. Duchambon, Y. Blouquit, and D. Lavalette. 2005. Disentangling ligand migration and heme pocket relaxation in cytochrome P450(cam). *Biophys. J.* 88:1250–1263.
9. Tetreau, C., M. Tourbez, A. Gorren, B. Mayer, and D. Lavalette. 1999. Dynamics of carbon monoxide binding with neuronal nitric oxide synthase. *Biochemistry.* 38:7210–7218.
10. Lavalette, D., and C. Tetreau. 1988. Viscosity-dependent energy barriers and equilibrium conformational fluctuations in oxygen recombination with hemerythrin. *Eur. J. Biochem.* 177:97–108.
11. Ehrenstein, D., and G. U. Nienhaus. 1992. Conformational substates in azurin. *Proc. Natl. Acad. Sci. USA.* 89:9681–9685.
12. Blumenfeld, L. A., R. M. Davydov, S. N. Magonov, and R. O. Vilu. 1974. Studies on the conformational changes of metalloproteins induced by electrons in water-ethylene glycol solutions at low temperatures. Cytochrome *c*. *FEBS Lett.* 45:256–258.
13. Blumenfeld, L. A., R. M. Davydov, S. N. Magonov, and R. O. Vilu. 1974. Studies on the conformational changes of metalloproteins induced by electrons in water-ethylene glycol solutions at low temperatures. Haemoglobin. *FEBS Lett.* 49:246–249.
14. Symons, M. C. R., and R. L. Petersen. 1978. Electron-capture by oxyhemoglobin—ESR study. *P. Roy. Soc. Lond. B. Bio.* 201:285–300.
15. Symons, M. C. R., and R. L. Petersen. 1978. The relative electron affinities of the alpha and beta chains of oxyhaemoglobin as a function of pH and added inositol hexaphosphate. An electron spin resonance study. *Biochim. Biophys. Acta.* 537:70–76.
16. Gasyna, Z. 1979. Intermediate spin-states in one-electron reduction of oxygen-hemoprotein complexes at low temperature. *FEBS Lett.* 106: 213–218.
17. Davydov, R., V. Kofman, H. Fujii, T. Yoshida, M. Ikedo-Saito, and B. Hoffman. 2002. Catalytic mechanism of heme oxidase through EPR and ENDOR of cryoreduced oxy-heme oxygenase and its Asp 140 mutants. *J. Am. Chem. Soc.* 124:1798–1808.
18. Davydov, R., T. Matsui, H. Fujii, M. Ikeda-Saito, and B. M. Hoffman. 2003. Kinetic isotope effects on the rate-limiting step of heme oxygenase catalysis indicate concerted proton transfer/heme hydroxylation. *J. Am. Chem. Soc.* 125:16208–16209.
19. Davydov, R., V. Kofman, J. M. Nocek, R. W. Noble, H. Hui, and B. M. Hoffman. 2004. Conformational substates of the oxyheme centers in alpha and beta subunits of hemoglobin as disclosed by EPR and ENDOR studies of cryoreduced protein. *Biochemistry.* 43:6330–6338.
20. Davydov, R., R. Perera, S. Jin, T.-C. Yang, T. A. Bryson, M. Sono, J. H. Dawson, and B. M. Hoffman. 2005. Substrate modulation of the properties and reactivity of the oxy-ferrous and hydroperoxo-ferric intermediates of cytochrome P450cam as shown by cryoreduction-EPR/ENDOR spectroscopy. *J. Am. Chem. Soc.* 127:1403–1413.
21. Blumenfeld, L. A., D. S. Burbaev, R. M. Davydov, L. N. Kubrina, A. F. Vanin, and R. O. Vilu. 1975. Studies on the conformational changes of metalloproteins induced by electrons in water-ethylene glycol solutions at low temperatures III. Adrenal ferredoxin. *Biochim. Biophys. Acta.* 379: 512–516.
22. Ericson, A., B. Hedman, K. O. Hodgson, J. Green, H. Dalton, J. G. Bentsen, R. H. Beer, and S. J. Lippard. 1988. Structural characterization by EXAFS spectroscopy of the binuclear iron center in protein A of methane monooxygenase from *Methylococcus capsulatus* (Bath). *J. Am. Chem. Soc.* 110:2330–2332.
23. De Witt, J. G., J. G. Bentsen, A. C. Rosenzweig, B. Hedman, J. Green, S. Pilkington, G. C. Papaefthymiou, H. Dalton, K. O. Hodgson, and S. J. Lippard. 1991. X-ray absorption, Mössbauer, and EPR studies of the dinuclear iron center in the hydroxylase component of methane monooxygenase. *J. Am. Chem. Soc.* 113:9219–9235.
24. Davydov, R., S. Kuprin, A. Gräslund, and A. Ehrenberg. 1994. Electron resonance study of the mixed-valent diiron center in *Escherichia coli* ribonucleotide reductase produced by reduction of radical-free protein R2 at 77 K. *J. Am. Chem. Soc.* 116:11120–11128.
25. Valentine, A. M., P. Tavares, A. S. Pereira, R. Davydov, C. Krebs, B. M. Hoffman, D. E. Edmondson, B. H. Huynh, and S. J. Lippard. 1998. Generation of a mixed-valent Fe(III)Fe(IV) form of intermediate

Q in the reaction of soluble methane monooxygenase, an analog of intermediate X in ribonucleotide reductase R2 assembly. *J. Am. Chem. Soc.* 120:2190–2191.

26. Lukoyanov, D., B. M. Barney, D. R. Dean, L. C. Seefeldt, and B. M. Hoffman. 2007. Connecting nitrogenase intermediates with the kinetic scheme for N2 reduction by a relaxation protocol and identification of the N2 binding state. *Proc. Natl. Acad. Sci. USA.* 104:1451–1455.
27. Hubbard, T. J. P., B. Ailey, S. E. Brenner, A. G. Murzin, and C. Chothia. 1999. SCOP: a structural classification of proteins database. *Nucleic Acids Res.* 27:254–256.
28. Sun, L., and K. Warncke. 2006. Comparative model of EutB from coenzyme B12-dependent ethanolamine ammonia-lyase reveals a b8a8, TIM-barrel fold and radical catalytic site structural features. *Proteins.* 64:308–319.
29. Bandarian, V., and G. H. Reed. 1999. Ethanolamine ammonia-lyase. *In* Chemistry and Biochemistry of B12. R. Banerjee, editor. John Wiley and Sons, New York. 811–833.
30. Toraya, T. 2003. Radical Catalysis in coenzyme B12-dependent isomerization (eliminating) reactions. *Chem. Rev.* 103:2095–2127.
31. Brown, K. 2005. Chemistry and enzymology of vitamin B12. *Chem. Rev.* 105:2075–2149.
32. Warncke, K., J. C. Schmidt, and S. C. Ke. 2008. Identification of a rearranged-substrate, product radical intermediate and the contribution of a product radical trap in vitamin B12 coenzyme-dependent ethanolamine deaminase catalysis. *J. Am. Chem. Soc.* 130:6055.
33. Warncke, K., J. C. Schmidt, and S.-C. Ke. 1999. Identification of a rearranged-substrate, product radical intermediate and the contribution of a product radical trap in vitamin B12 coenzyme-dependent ethanolamine deaminase catalysis. *J. Am. Chem. Soc.* 121:10522–10528.
34. Sun, L., O. A. Groover, J. M. Canfield, and K. Warncke. 2008. Critical role of arginine 160 of the EutB protein subunit for active site structure and radical catalysis in coenzyme B12-dependent ethanolamine ammonia-lyase. *Biochemistry.* 47:5523–5535.
35. Babior, B. M., T. H. Moss, W. H. Orme-Johnson, and H. Beinert. 1974. The mechanism of action of ethanolamine ammonia lyase, a B12-dependent enzyme: The participation of paramagnetic species in the catalytic deamination of 2-aminopropanol. *J. Biol. Chem.* 249: 4537–4544.
36. Bandarian, V., and G. H. Reed. 2002. Analysis of the electron paramagnetic resonance spectrum of a radical intermediate in the coenyzme b12-dependent ethanolamine ammonia-lyase catalyzed reaction of S-2-aminopropanol. *Biochemistry.* 41:8580–8588.
37. Canfield, J. M., and K. Warncke. 2002. Geometry of reactant centers in the CO^{II}-substrate radical pair state of coenzyme B12-dependent ethanolamine deaminase determined by using orientation-selection-ESEEM spectroscopy. *J. Phys. Chem. B.* 106:8831–8841.
38. Weisblat, D. A., and B. M. Babior. 1971. The mechanism of action of ethanolamine ammonia-lyase, a B12-dependent enzyme. VIII. Further studies with compounds labelled with isotopes of hydrogen: Identification and some properties of the rate limiting step. *J. Biol. Chem.* 246:6064–6071.
39. Carty, T. J., B. M. Babior, and R. H. Abeles. 1974. The mechanism of action of ethanolamine ammonia-lyase, a B12-dependent enzyme. Evidence for two intermediates in the catalytic process. *J. Biol. Chem.* 249:1683–1688.
40. Poyner, R. R., M. A. Anderson, V. Bandarian, W. W. Clelland, and G. H. Reed. 2006. Probing nitrogen-sensitive steps in the free-radical-mediated deamination of amino alcohols by ethanolamine ammonia-lyase. *J. Am. Chem. Soc.* 128:7120–7121.
41. Licht, S. S., C. C. Lawrence, and J. Stubbe. 1999. Class II ribonucleotide reductases catalyze carbon-carbon bond reformation on every turnover. *J. Am. Chem. Soc.* 121:7463–7468.
42. Bradbeer, C. 1965. The clostridial fermentations of choline and ethanolamine. *J. Biol. Chem.* 240:4669–4674.
43. Faust, L. P., J. A. Connor, D. M. Roof, J. A. Hoch, and B. M. Babior. 1990. AdoCbl-dependent ethanolamine amino-lyase from *Salmonella typhimurium*. *J. Biol. Chem.* 265:12462–12466.
44. Faust, L. P., and B. M. Babior. 1992. Overexpression, purification and some properties of AdoCbl-dependent ethanolamine amino-lyase from *Salmonella typhimurium*. *Arch. Biochem. Biophys.* 294:50–54.
45. Harkins, T., and C. B. Grissom. 1995. *J. Am. Chem. Soc.* 117:566–567.
46. Kaplan, B. H., and E. R. Stadtman. 1968. Ethanolamine deaminase, a cobamide coenzyme-dependent enzyme. *J. Biol. Chem.* 243:1787–1793.
47. Hollaway, M. R., A. W. Johnson, M. F. Lappert, and O. C. Wallis. 1980. The number of functional sites per molecule of the adenosylcobalamin-dependent enzyme, ethanolamine deaminase, as determined by a kinetic method. *Eur. J. Biochem.* 111:177–188.
48. Bandarian, V., and G. H. Reed. 1999. Hydrazine cation radical in the active site of ethanolamine ammonia-lyase: mechanism-based inactivation by hydroxyethylhydrazine. *Biochemistry.* 38:12394–12402.
49. Moore, J. W., and R. G. Pearson. 1981. Kinetics and Mechanism. Wiley and Sons, New York.
50. Pilbrow, J. R. 1982. EPR of B12-dependent enzyme reactions and related systems. *In* B12. D. Dolphin, editor. Wiley, New York. 431–462.
51. Boas, J. F., P. R. Hicks, J. R. Pilbrow, and T. D. Smith. 1978. Interpretation of electron spin resonance spectra due to some B12-dependent enzyme reactions. *J. Chem. Soc. Faraday II.* 74:417–431.
52. Canfield, J. M., and K. Warncke. 2005. Active site reactant center geometry in the CO^{II}-product radical pair state of coenzyme B12-dependent ethanolamine deaminase determined by using orientation-selection-ESEEM spectroscopy. *J. Phys. Chem. B.* 109:3053–3064.
53. Ke, S.-C. 2003. Spin-spin interaction in ethanolamine deaminase. *Biochim. Biophys. Acta.* 1620:267–272.
54. Wetmore, S. D., D. M. Smith, J. T. Bennett, and L. Radom. 2002. Understanding the mechanism of action of B12-dependent ethanolamine ammonia-lyase: synergistic interactions at play. *J. Am. Chem. Soc.* 124:14054–14065.
55. Semialjac, M., and H. Schwarz. 2003. Computational study on mechanistic details of the aminoethanol rearrangement catalyzed by the vitamin B12-dependent ethanolamine ammonia lyase: His and Asp/Glu acting simultaneously as catalytic auxiliaries. *J. Org. Chem.* 68:6967–6983.
56. Sandala, G. M., D. M. Smith, and L. Radom. 2005. Divergent mechanisms of suicide inactivation for ethanolamine ammonia-lyase. *J. Am. Chem. Soc.* 127:8856–8864.
57. Wang, M., and K. Warncke. 2008. Kinetic and thermodynamic characterization of CO^{II}-substrate radical pair formation in coenzyme B12-dependent ethanolamine ammonia-lyase in a cryosolvent system by using time-resolved, full-spectrum continuous-wave electron paramagnetic resonance spectroscopy. *J. Am. Chem. Soc.* 130:4846–4858.
58. Tang, K.-H., C. H. Chang, and P. A. Frey. 2001. Electron transfer in the substrate-dependent suicide inactivation of lysine 5,6-aminomutase. *Biochemistry.* 40:5190–5199.
59. Magnusson, O. T., and P. A. Frey. 2002. Interactions of diol dehydrase and 3′-4′-anhydroadenosylcobalamin: suicide inactivation by electron transfer. *Biochemistry.* 41:1695–1702.
60. Huhta, M. S., D. Ciceri, B. T. Golding, and E. N. G. Marsh. 2002. A novel reaction between adenosylcobalamin and 2-methyleneglutarate catalyzed by glutamate mutase. *Biochemistry.* 41:3200–3206.
61. Vlasie, M. D., and R. Banerjee. 2004. When a spectator turns killer: suicidal electron transfer from cobalamin in methylmalonyl-CoA mutase. *Biochemistry.* 43:8410–8417.
62. Chen, E., and M. R. Chance. 1993. Continuous-wave quantum yields of various cobalamins are influenced by competition between geminate recombination and cage escape. *Biochemistry.* 32:1480–1487.
63. Bandarian, V., and G. H. Reed. 2000. Isotope effects in the transient phases of the reaction catalyzed by ethanolamine ammonia-lyase: determination of the number of exchangeable hydrogens in the enzyme-cofactor complex. *Biochemistry.* 39:12069–12075.

64. Holloway, M. R., H. A. White, K. N. Joblin, A. W. Johnson, M. F. Lappert, and C. O. Wallis. 1978. A spectrophotometric rapid kinetic study of reactions catalyzed by coenzyme B12-dependent ethanolamine ammonia-lyase. *Eur. J. Biochem.* 82:143–154.

65. Wallis, O. C., R. C. Bray, S. Gutteridge, and M. R. Hollaway. 1982. The extents of formation of cobalt(II)-radical intermediates in the reactions with different substrates catalyzed by the adenosylcobalamin-dependent enzyme ethanolamine ammonia-lyase. *Eur. J. Biochem.* 125: 299–303.

66. Angell, C. A. 1995. Formation of glasses from liquid and biopolymers. *Science.* 267:1924–1935.

67. Ringe, D., and G. A. Petsko. 2003. The 'glass transition' in protein dynamics: what it is, why it occurs, and how to exploit it. *Biophys. Chem.* 105:667–680.

68. Ke, S.-C., M. Torrent, D. G. Museav, K. Morokuma, and K. Warncke. 1999. Identification of dimethylbenzimidazole axial coordination and characterization of 14N superhyperfine and nuclear quadrupole coupling in Cob(II)alamin bound to ethanolamine deaminase in a catalytically-engaged substrate radical-CO^{II} biradical state. *Biochemistry.* 38:12681–12689.

69. Abend, A., V. Bandarian, R. Nitsche, E. Stupperich, J. Retey, and G. H. Reed. 1999. Ethanolamine ammonia-lyase has a ''base-on'' binding mode for coenzyme B12. *Arch. Biochem. Biophys.* 370:138–141.